A Quantitative Coarse-Grain Model for Lipid Bilayers

Mario Orsi,[‡] David Y. Haubertin,[‡] Wendy E. Sanderson,[†] and Jonathan W. Essex*[,‡]

School of Chemistry, University of Southampton, Southampton, SO17 1BJ United Kingdom, and Johnson & Johnson PRD, Janssen Pharmaceutica NV, Beerse, 2340 Belgium

Received: August 1, 2007; In Final Form: September 14, 2007

A simplified particle-based computer model for hydrated phospholipid bilayers has been developed and applied to quantitatively predict the major physical features of fluid-phase biomembranes. Compared with available coarse-grain methods, three novel aspects are introduced. First, the main electrostatic features of the system are incorporated explicitly via charges and dipoles. Second, water is accurately (yet efficiently) described, on an individual level, by the soft sticky dipole model. Third, hydrocarbon tails are modeled using the anisotropic Gay−Berne potential. Simulations are conducted by rigid-body molecular dynamics. Our technique proves 2 orders of magnitude less demanding of computational resources than traditional atomic-level methodology. Self-assembled bilayers quantitatively reproduce experimental observables such as electron density, compressibility moduli, dipole potential, lipid diffusion, and water permeability. The lateral pressure profile has been calculated, along with the elastic curvature constants of the Helfrich expression for the membrane bending energy; results are consistent with experimental estimates and atomic-level simulation data. Several of the results presented have been obtained for the first time using a coarse-grain method. Our model is also directly compatible with atomic-level force fields, allowing mixed systems to be simulated in a multiscale fashion.

Introduction

Lipid bilayers are complex and fascinating systems; they are characterized by highly heterogeneous structure and dynamics, and display an astonishingly rich and biologically relevant behavior on a vast range of spatial and temporal scales.[1−3] Experimental investigation of the physics of membranes allows the determination of a large body of bilayer features. The internal structure can be described via electron density profiles,[4] the ordering of the hydrocarbon tails is quantified by order parameters,[5] fluidity is studied by lateral diffusion measurements,[6] mechanical properties can be related to the measurements of elastic moduli,[7] electrostatic properties are quantified by estimating internal potentials,[8] and even the transbilayer pressure distribution can be qualitatively measured.[9] These fundamental membrane properties are central to an incredibly large number of biological mechanisms. The bilayer structure directly influences the conformation of embedded proteins, whereas lipid fluidity is crucial, for example, for membrane lateral organization. The membrane dipole potential and associated electric field also play fundamental roles; for example, they are involved in the regulation of membrane proteins, membrane fusion, insertion and folding of amphiphilic peptides, redox reactions, permeability, interaction with drugs, and signaling.[10] An even more important feature is the lateral pressure profile, which characterizes the transmembrane distribution of forces. The lateral pressure profile is the most fundamental physical property of lipid bilayers;[3] it determines the interfacial area, it is at the basis of phase transitions and fusion,[11] it modulates the insertion, folding, and functioning of membrane proteins,[12] and it affects permeability,[13] drug transport,[14] and anesthesia.[15] The lateral pressure profile is also directly related to the elastic curvature constants that characterize the Helfrich expression for the bending free energy.[16−18] These constants, in turn, control membrane shape and play specific roles in the mechanisms modulated by the lateral pressure profile.

Considering the amount and variety of phenomena associated with lipid bilayers, it is clear that the development of realistic models is a delicate and challenging task. Particle-based computer simulation represents a powerful tool to model biomembranes, as it can provide detailed dynamic and thermodynamic data for a broad range of systems.

Atomic-level (AL) models have been employed for decades now and have significantly contributed to the understanding of many membrane phenomena.[19−36] However, AL methods require an enormous amount of computational resources to calculate the interactions between all atoms in the system. The large computational cost of AL models results in a number of limitations and issues. For example, collective, large-scale phenomena such as self-assembly, membrane fusion, or microdomain formation (lipid rafts) are typically intractable. In fact, apart from one exception,[20] all published AL simulations to date have been carried out on preassembled bilayers due to the prohibitive computational cost of simulating self-assembly; this does not guarantee that the system is at thermodynamic equilibrium. Furthermore, the reliability of the calculation of some important properties, such as the lipid area, diffusion coefficients, or the lateral pressure profile, can be undermined by insufficient sampling. These issues can be tackled by adopting a simplified, coarse-grain description.

The coarse-grain (CG) methodology generally involves grouping together selected clusters of atoms into single macrosites to significantly reduce the number of interactions calculated and, hence, also the computational cost. Over the past few years, the CG field has grown significantly; a large number of models have been developed for different membrane

* To whom correspondence should be addressed. Tel.: +44 (0)23 8059 2794. Fax: +44 (0)23 8059 3781. E-mail: j.w.essex@soton.ac.uk.
‡ University of Southampton.
† Janssen Pharmaceutica NV.

10.1021/jp076139e CCC: $40.75
Published on Web 12/18/2007

systems and with differing degrees of simplification.[37−39] We now review those CG models of phospholipid membranes that retain an explicit connection with the chemical identity of the systems described, as this is the level at which our new methodology is located. Such models can be called "specific". In the specific CG models,[40−45] a lipid molecule, which at the atomic level comprises about 100 particles, is typically reduced to around 10 CG sites. To further increase simulation efficiency, the representations of water and electrostatics are highly simplified. A popular strategy involves representing three[42−44] or four[40] water molecules as single CG units. However, in one model,[45] water molecules are described individually, whereas in another,[41] solvation is described implicitly. None of these models explicitly includes water electrostatics. The charges in the lipid glycerol−ester region are also not explicitly represented. As for the lipid headgroup region, electrostatics are present in most models, where, however, artificial dielectric constants are introduced to account for water screening.[40−43] Such simple models can be orders of magnitude more efficient than corresponding AL systems, and hence, they can be applied to simulate phenomena at larger temporal and spatial scales, such as self-assembly,[40−42,46] phase transition,[47,48] and vesicle fusion.[49] CG simulations have also been conducted to study the interaction with inclusions such as alcohols,[50] anesthetics,[51] cholesterol,[52] and even proteins.[53] These studies are interesting because they have given access to membrane processes that are difficult to investigate by any other theoretical or experimental technique. However, we have identified a number of issues in these CG models and their application. The oversimplification[40−43] or lack[44,45] of explicit electrostatics inherently precludes an accurate representation of charge-dependent properties. The membrane dipole potential, electric field, and orientational polarization effects cannot be modeled; related phenomena might be ill-represented. The highly simplified modeling of water as a rather generic, apolar solvent is also a matter of concern. Water is a fundamental component of membrane systems; it drives the formation of lipid aggregates through the hydrophobic effect and provides the necessary electrostatic screening between charged particles (such as headgroups and ions). These features are not consistently accounted for by the referenced CG models. Water also generates a significant electric field by collectively orienting its dipoles; clearly, such a local polarization effect cannot be captured by apolar solvent particles. Other issues affecting the specific CG models developed to date involve the membrane dynamic properties, which are reproduced with some difficulty, and the associated issue in interpreting the simulation time scales. For example, lipid diffusion coefficients have been reported to be 4[40,52] to 100[46] times higher than experimental data; as already pointed out elsewhere,[54] the ad hoc rescaling of the simulation time according to these factors[40,46] is questionable because it assumes that all dynamic events are homogeneous in time scale, whereas, in general, dynamic processes in membrane systems are highly heterogeneous. Another issue concerns the attractive possibility of mixing CG and AL representations in multiscale simulation, where selected parts of the system are described at an atomic level, whereas the surrounding environment is simulated by simplified models. It would not be straightforward to interface the available CG models with AL representations due to the radically different description of electrostatics and solvent. An original approach to the problem involves performing a rigorous and consistent parametrization of the mixed AL−CG interactions,[55] although charges are still absent.

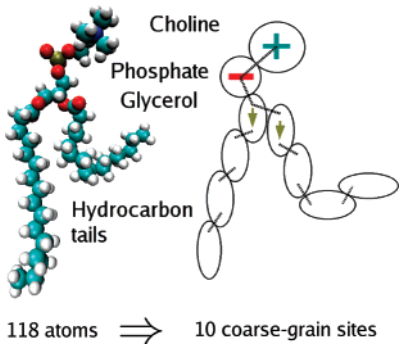

Figure 1. Lipid coarse-graining strategy. The left molecule is an all-atom representation of a DMPC lipid. The corresponding CG model is depicted on the right. CG electrostatics are highlighted; they comprise positive ("+" sign) and negative ("−" sign) point charges and point dipoles (arrows). Harmonic springs, representing CG covalent bonding, are also shown (dotted lines).

In this article, we present a new specific CG model that addresses the issues discussed above. In common with the models reviewed, we have significantly simplified the representation of lipid molecules to increase simulation efficiency. In contrast to the other models, we have retained an explicit description of water and the major electrostatics. The model characteristics are described in the following section, along with the simulation methodology and the parametrization procedure. The predictive power of our new CG model will then be demonstrated by reproducing experimental observables against which it is not directly fitted. All major physical properties of fluid-phase phospholipid bilayers will be investigated; many of these properties are reproduced for the first time using a CG method. Moreover, the force field developed will be shown to be directly compatible with AL representations. Model extensions, and preliminary applications in the context of multiscale simulation, will be discussed.

Methodology

Lipid Model. We have designed a CG model for dimyristoylphosphatidylcholine (DMPC); Figure 1 shows both the AL structure and our simplified CG representation. Each lipid molecule, in reality comprising more than 100 atoms, has been reduced to 10 macrounits. The lipid headgroup is coarse-grained into two Lennard-Jones spherical units, accounting for the choline and phosphate moieties. Headgroup electrostatics are represented by a positive point charge embedded in the choline group and a negative one in the phosphate group. The glycerol and hydrocarbon regions are modeled by soft uniaxial ellipsoids through the Gay−Berne potential.[56] The Gay−Berne potential can be seen as an extension of the (isotropic) Lennard-Jones potential, where extra terms are included to allow the modeling of nonspherical (anisotropic) particles. In particular, the glycerol−ester region is described by two Gay−Berne ellipsoidal units, each embedded with a point dipole to account for the dipolar charge distribution in this region. Hydrocarbon tails are modeled by chains of three neutral Gay−Berne ellipsoids, each representing a segment of four consecutive methyl groups. The shape of the Gay−Berne ellipsoids can be tuned to accurately capture the underlying real elongated structure of the tail segments considered. We have already used the Gay−Berne representation of lipid tails to simulate an idealized bilayer, without headgroups and solvation; despite the simplicity of that model, order parameters and diffusion coefficients proved consistent with experiment.[57] Mixed Lennard-Jones/Gay−Berne interactions (between headgroup and tail sites) are consistently treated using

the generalized Gay−Berne potential.[58] Explicit formulas of potentials, forces, and torques for both the original Gay−Berne model and its generalized version are reported in detail elsewhere.[56,58,59] Intralipid bonds are modeled by the Hooke potential, as is standard practice. No angle or torsional potentials are present.

Water Model. Water molecules are represented by the soft sticky dipole (SSD) model.[60] The SSD water is a single-site model; the three atoms of individual water molecules are coarse-grained into a single interaction center, which comprises a Lennard-Jones core providing excluded volume, a point dipole to account for electrostatics, and a tetrahedral "sticky" term to model hydrogen bonding. Detailed formulas of the SSD potential, and corresponding forces and torques, can be found elsewhere.[60,61] The SSD model is about 1 order of magnitude computationally cheaper than the traditional AL multisite water models, yet it accurately reproduces structural, thermodynamic, dielectric, dynamic, and temperature-dependent properties.[60−63] The Lennard-Jones term of the SSD potential interacts with the Gay−Berne lipid terms (tail and glycerol sites) through the generalized Gay−Berne potential.[58]

Treatment of Electrostatics. All electrostatic terms in our model interact with each other through either charge−charge, charge−dipole, or dipole−dipole potentials.[64] A relative dielectric constant $\epsilon_r = 1$ is assumed, that is, no artificial explicit screening is introduced. Long-range electrostatics are treated using cutoff schemes. In particular, charge−charge and charge−dipole interactions are implemented using the shifted-force cutoff method.[65] We employ the SSD parameters optimized to treat long-range dipole−dipole interactions with a cubic switching cutoff scheme;[62] for consistency, all dipole−dipole interactions are treated in this manner. We are aware that using cutoffs to approximate long-range electrostatics might introduce simulation artifacts. In AL simulation, long-range electrostatic interactions are typically included by Ewald techniques,[66] which however are also known to introduce artifacts.[67−70] In fact, it has been argued that cutoff schemes can be as good as[69] or better[70] than Ewald methods. We have chosen the cutoff alternative as its simplicity and efficiency are consistent with the overall spirit of simplification of the model.

Simulation Details. To study our model by molecular dynamics, we have specifically developed the software BRAHMS.[71] The basic structure of BRAHMS has been designed following Rapaport.[72] Interactions are computed using a combined cell-subdivision/neighbor-list algorithm, which relies on standard periodic boundary and minimum image conventions. Dedicated routines have been implemented for the calculation of energies, forces, and torques, the integration of rigid-body dynamics, the control of pressure and temperature, as well as for the analysis of the trajectory. The translational motion of all particles is described by Newton's second law. Lennard-Jones particles (lipid headgroups) are represented as point masses, their position being defined by the coordinates of the mass centers, as is standard practice. Gay−Berne particles (lipid tails) are represented as symmetric rigid bodies, whereas SSD molecules (water) are represented as general, nonsymmetric rigid bodies; the rotational motion is described by Euler's equation, the orientations being represented with rotation matrices. To numerically integrate the equations of motion, we have implemented an advanced symplectic and time-reversible method.[73] The initial membrane configuration was constructed from a set of AL coordinates for hydrated DMPC.[74] Groups of atoms were mapped into CG interaction sites according to our CG strategy (Figure 1). The number of water molecules was adjusted to match the experimental hydration level of 26.6 water/lipid.[4] Our final system comprises 128 DMPC lipids and 3400 water molecules. Coordinates are defined in a Cartesian frame with the origin in the center of the simulation region; the x and y axes lie parallel to the bilayer interfacial plane, the z axis thus being perpendicular to it. The z axis will also be referred to as the (interfacial) "normal". Molecular dynamics simulations are carried out with an integration time step of 20 fs. This time step is larger than those normally employed in AL simulation (1−5 fs), and hence, it allows more efficient sampling. This improvement is determined by the removal of fast degrees of freedom (such as those, typical in AL models, due to stiff harmonic potentials or light particles) and the excellent stability properties of the integration algorithm implemented.[73] Pressure and temperature are maintained at 1 atm and 30 °C using the weak-coupling scheme.[75] Lipid and water temperatures are coupled separately with a time constant of $\tau_T = 0.2$ ps; for rigid-body sites, translational and rotational degrees of freedom are coupled independently. The pressure is controlled by semi-isotropic volume scaling, with a time constant of $\tau_P = 0.5$ ps and an isothermal compressibility of $\beta = 4.6 \times 10^{-5}$ atm^{-1}. The cutoff radius for both Lennard-Jones and electrostatic water−water interactions is 0.9 nm.[62] All other nonbonded cutoff radii, both for Lennard-Jones and electrostatic interactions, are set to 1.2 nm. The net mass center velocity of the entire system is set to zero at every step.[76] To avoid artifacts in the evaluation of lipid diffusion,[23] the net lateral translation of each of the two monolayers is removed at every step.

Sampling Enhancement. To estimate the efficiency gain of our simplified CG methodology over traditional AL modeling, we compared the sampling speed of our code BRAHMS with the popular AL software CHARMM.[77] We selected an AL test system[26] and constructed a corresponding CG configuration; both membranes comprised 72 lipids and 2094 water molecules. In particular, there were 2814 interaction sites in the CG system and 15210 atoms in the AL system. Our model was simulated with a 20 fs time step and cutoff treatment of long-range interactions, whereas the AL simulation was conducted with a 2 fs time step and PME scheme[66] for evaluation of long-range electrostatics. By simulating on the same AMD 1400 MHz processor, we measured sampling speeds of 324 ps/CPU-hour for BRAHMS and 2.5 ps/CPU-hour for CHARMM, corresponding to a CG speed-up factor of ≈130. The choice of a 2 fs time step in the AL run is typical for AL membrane simulations.[19,26−32,34−36] We are aware that the use of constraint and multistep algorithms can allow time steps of 4[21,22] and even 5 fs,[20,23] hence more than twice larger than that employed in our test. Using a 5 fs time step in the AL run would bring the CG speed-up factor down to ≈50. However, there are also some AL membrane studies that report the use of a 1 fs time step.[24,25,33] Overall, our choice to consider an "average" AL time-step of 2 fs seems reasonable. We are also aware that the reported CG speed-up factor benefits, in part, from the cutoff treatment of CG electrostatic interactions with respect to the more costly PME scheme used in the AL CHARMM simulation. Also, CHARMM is not the most efficient biological molecular dynamics code; however, significant effort has not been made to optimize the performance of BRAHMS. In summary, it seems acceptable to claim that the reduced number of interactions, the use of larger integration time steps, and the simplified treatment of electrostatics make our CG technique roughly 2 orders of magnitude less demanding of computational resources than traditional AL methodology. All data reported in the rest of the paper refer to the larger membrane (128 DMPC lipids and 3400

water molecules) described in the previous section; single-processor simulations of this system have been carried out on the Iridis high-performance computational cluster at the University of Southampton,[78] where BRAHMS runs at up to 22 ns/CPU-day.

Force Field Parametrization. We chose to parametrize the CG force field of our lipid model to reproduce the experimental volume and area per lipid[4] and the average segmental tail order parameter[5,79] of fluid-phase DMPC. The volume per lipid is computed as $V_L = (V_T - N_W V_W)/N_L$, with V_T as the total volume of the system, N_W as the number of water molecules, V_W as the volume per water, and N_L as the number of lipids. The area per lipid is computed as $A_L = A/N_L^m$, with A as the total interfacial area and N_L^m as the number of lipids per monolayer. Second-rank order parameters are calculated for the CG tail sites as $(3\cos^2\theta - 1)/2$, with θ being the angle between the ellipsoid axis and the bilayer normal. The six tail ellipsoids of each lipid are sorted, in pairs, into three layers at different depths along the tails; the "top layer" comprises the tail sites connected to the glycerol units, the "end layer" comprises the terminal tail sites, and the "midlayer" is between the previous two. We compute segmental order parameters for each of the three layers so defined and the average order parameter for the entire hydrocarbon tail region.

Setting of Bond Rigidity, Masses, and Moments of Inertia. The rigidity constant of the Hooke potential, modeling intralipid covalent bonds as harmonic springs, is set to 3 kcal/(mol Å^2), a typical value for CG models.[40] The reference bond lengths are set to zero for simplicity, although they could have also been empirically assigned. Both approaches seem equally reasonable, as the CG springs are extremely soft; the selected CG rigidity constant is 2 orders of magnitude smaller than those normally used for AL bond stretching (300−800 kcal/(mol Å^2)).[80] The masses of the CG lipid sites are set to the sum of the atomic masses of the corresponding AL groups. For the ellipsoidal rigid-body units, the principal moments of inertia are assigned assuming uniform density. The mass and principal moments of inertia of water sites are increased to optimize the stability of molecular dynamics integration.[81] In particular, the water mass is set to 50 amu (the real value being 18 amu). The chosen principal moments of inertia correspond to a redistribution of water masses as follows: 15 amu for each hydrogen and 20 amu for the oxygen. Thermodynamic properties are not affected by such an alteration of the inertial features of water. However, dynamics are intuitively predicted to be somewhat slower. To quantify this effect, we ran a simulation of a pure water system comprising 500 molecules and computed the diffusion coefficient. Our result of 1.8×10^{-5} cm^2/s is only slightly lower than the experimental value[82] of 2.3×10^{-5} cm^2/s, indicating that the dynamic behavior of our "heavy" water remains realistic.

Nonbonded Terms: Initial Setting and Refinement. Preliminary Lennard-Jones parameters for the headgroup sites were set by fitting the potential energy of the CG sites to that of the corresponding AL clusters of particles. Gay−Berne parameters were initially taken from our previous model of the hydrocarbon tails.[57] Lennard-Jones and Gay−Berne cross terms are calculated by standard rules,[58,65] with the following exceptions, where scaling factors are introduced: (i) To promote the self-assembly process, the mixed Lennard-Jones/Gay−Berne energy parameters between hydrophilic (water and headgroup) and hydrophobic (tail) sites are decreased. (ii) To mimic the hydrogen-bonding capabilities of phosphate−water and glycerol−water pairs, the corresponding Lennard-Jones/Gay−Berne energy cross terms are increased. The magnitudes of the headgroup charges and glycerol dipoles have been chosen to reproduce the corresponding net charges and dipoles computed from the underlying AL distribution of partial charges. Initial simulations were performed on a preassembled bilayer. Parameters were optimized by trial-and-error molecular dynamics to reproduce the targeted experimental data. In each trial-and-error simulation, the area per lipid (which is the slowest-converging quantity) typically reached equilibrium in ≈20 ns, corresponding to one CPU-day of simulation with BRAHMS. By running several tests in parallel, the parameter space could be explored quite efficiently. The experimental volume and area per lipid could be matched by tuning the Lennard-Jones parameters of the headgroup particles, whereas tail order parameters were reproduced by adjusting the Gay−Berne potential. Self-assembly runs were then prepared. To generate an initial random solution of lipids and water, the preassembled bilayer was brought to high temperature (up to 1000 °C) while switching off electrostatics; runs were continued until visual inspection and order parameters confirmed a completely random configuration. By varying the temperature and the run length, several different starting configurations were obtained (typically, less than 1 CPU-hour of simulation is sufficient for each "disassembling" run). We then restored the electrostatics and started the self-assembly simulations at a temperature of 30 °C; self-aggregation was typically completed over a time scale of ≈100 ns. Further trial-and-error runs were carried out to refine the force field until we consistently obtained stable, defect-free bilayers matching the targeted experimental structural properties. The final complete parameter set is reported in Table 1; standard naming conventions are employed for the potentials, namely, Lennard-Jones,[65] Gay−Berne,[56] generalized Gay−Berne/Lennard-Jones,[58] electrostatic,[64] and Hooke.[80]

Fitted Properties. Snapshots from a representative self-assembly simulation are displayed in Figure 2. A fast phase separation between lipids and water is followed by a slow rearrangement of the bilayer to expose the headgroups while burying the hydrocarbon tails in the interior. A transient water pore is also observed. The time scale and the overall aggregation mechanism are consistent with the only AL self-assembly simulation reported to date.[20] We then analyzed the self-assembled bilayers to check the correct reproduction of the targeted experimental data. The time evolution of the lipid volume V_L and area A_L over a 100 ns time window (after self-assembly) is shown in Figure 3, together with the experimental estimates. Our measurements $V_L = 1.104 \pm 0.002$ nm^3 and $A_L = 0.594 \pm 0.003$ nm^2 are consistent with the experimental data[4] $V_L = 1.101$nm^3 and $A_L = 0.606$ nm^2. The fluctuations are similar to those observed with AL models.[21,23] Segmental order parameters for the three layers previously defined are plotted in Figure 4, along with the experimental data. The agreement is rather good, apart from the midlayer order parameter, which is somewhat lower than the experimental values. We calculated an average segmental order parameter for the entire tail region of $S_{mol} = 0.36 \pm 0.01$, consistent with the value of 0.38 deduced from the experimental data.[5,79] Standard errors have been estimated using the block averaging method[72] using 10 consecutive 10 ns blocks.

Results

In this section, we thoroughly investigate the physical properties of our self-assembled CG bilayer model. Simulation results will be primarily compared to experimental data, although in some cases, AL and CG models, and alternative theoretical

TABLE 1: Force Field Parameters[a]

parameter	value
σ_{CC}	5.0 Å
σ_{PP}	4.9 Å
σ_{GG}	3.8 Å
σ_{TT}	3.8 Å
σ_{WW}	3.035 Å
ϵ_{CC}	1.9 kcal/mol
ϵ_{PP}	2.0 kcal/mol
ϵ_{GG}	1.3 kcal/mol
ϵ_{TT}	1.3 kcal/mol
ϵ_{WW}	0.152 kcal/mol
ϵ_{TW}	$\sqrt{\epsilon_{TT}\epsilon_{WW}}/3$
ϵ_{TC}	$\sqrt{\epsilon_{TT}\epsilon_{CC}}/2$
ϵ_{TP}	$\sqrt{\epsilon_{TP}\epsilon_{PP}}/2$
ϵ_{WP}	$1.5\sqrt{\epsilon_{WW}\epsilon_{PP}}$
ϵ_{WG}	$1.5\sqrt{\epsilon_{WW}\epsilon_{GG}}$
μ	2
ν	1
κ	1.77
κ'	20
Q_C	+0.7e
Q_P	−0.7e
μ_G	3 D
μ_W	2.42 D
k	3 kcal/(mol Å^2)

[a] Subscripts C, P, G, T, and W stand for the site types choline, phosphate, glycerol, tail, and water, respectively. Lennard-Jones cross terms are calculated by a standard rule,[65] except for ϵ_{TW}, ϵ_{TC}, ϵ_{TP}, ϵ_{WP}, and ϵ_{WG}, which have been set as reported. The constants μ, ν, κ and κ' refer to Gay−Berne parameters.[56] As for the mixed Gay−Berne/Lennard-Jones potential,[58] cross terms $\chi\alpha^{-2}$ are calculated by a standard rule,[58] and $\chi'\alpha'^{-2} = 0$. Charges and dipoles are identified by Q and μ; cross terms are obtained via a standard rule.[64] The rigidity of the Hooke spring potential is identified by k; reference lengths are zero. Springs are anchored at the mass center for C and P sites and at a distance of $\kappa_{GB}\sigma_{TT}/4$ from the mass center along the symmetry axes for G and T sites.

approaches, will also be considered. If not otherwise stated, all data reported for comparison refer to systems and conditions consistent with our simulations, that is, fully hydrated liquid-phase DMPC bilayers at 30 °C. We simulated a self-assembled bilayer for several hundreds of nanoseconds, over which time the system remained stable and all of the properties observed fluctuated around their equilibrium values. Most of the measurements were taken over a 200 ns time window; for each parameter measured, the reported average value and standard error have been computed from two subaverages taken over the two 100 ns consecutive blocks of the trajectory, unless otherwise stated. However, to compute the water permeability coefficient, the detection of water permeation events was carried out for 900 ns; this long simulation time was necessary to collect enough statistics on such relatively rare events. The analysis of a number of properties was carried out following a general process that involves "slicing" the system along planes perpendicular to the z axis (interface normal). In particular, we have defined 600 slices of thickness $\Delta z \approx 0.1$ Å, the actual value of Δz being evaluated at every step to account for the fluctuations of the z dimension of the simulation region. Several bilayer properties are homogeneous inside of a particular slice due to the intrinsic axial symmetry of the system. Therefore, single curves, profiles evaluated as a function of z, provide full characterization. The slicing procedure was employed to calculate the following profiles: electron density, lateral pressure, electric field, water polarization, and electrostatic potential. We report the average profiles obtained from calculation at every molecular dynamics integration step over the 200 ns measurement time. No extra processing has been done, that is, no filters have been applied to smooth the curves, and we have not averaged over the two monolayers. It will be seen that the profiles are, nonetheless, extremely smooth (almost noise-free) and symmetrical. This is indicative of a well-equilibrated system and adequate sampling. We again emphasize that all properties considered in the following did not directly enter the parametrization process.

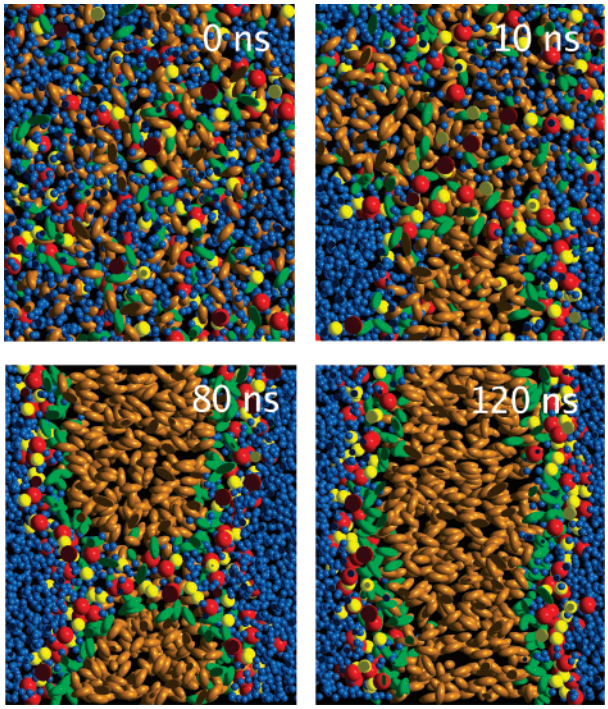

Figure 2. Self-assembly simulation snapshots. The choline, phosphate, glycerol, and tail sites of lipid molecules are represented in red, yellow, green, and orange, respectively. Water molecules are colored in blue. A quick phase separation (0−10 ns) is followed by the formation of a transient water pore (80 ns), which eventually disappears, leading to the stabilization of a defect-free bilayer (120 ns).

Structure. *Electron Density Profile.* In general, to estimate the electron distribution from particle-based models, electrons have to be arbitrarily assigned to each site. Care should be taken to match as closely as possible the underlying real electron locations, with the obvious requirement for the total number of electrons per lipid in the model to be equal to the real value (374 for DMPC). For our model, we assume all electrons belonging to the choline and phosphate clusters to be located at the mass center of the choline and phosphate CG units, respectively. As for the ellipsoidal particles that constitute the rest of the lipid in our representation, we have resolved four positions evenly spaced along the principal axis of each ellipsoid; electrons are assigned to these positions to match as closely as possible the underlying real distribution. The total electron density profile of our model is reported in Figure 5 along with the experimental profile;[4] the agreement is rather good. In fact, our profile matches the experimental result with an accuracy which is comparable to the results obtained with AL models.[22−24] The only significant difference involves the central region, corresponding to the terminal methyl groups, where the density of our model is slightly higher than that obtained from experiment. The pronounced central trough in the electron density is possibly determined by the "curling up" of the terminal methyl segment; experimental order parameters[5] indeed indicate that the terminal methyl segment is significantly tilted with respect to the neighboring segment. Our model (by

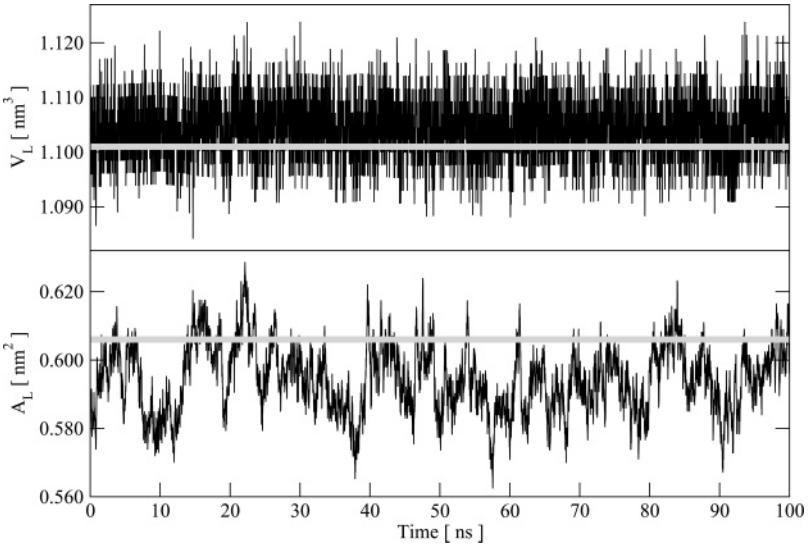

Figure 3. Time evolution of the volume V_L and the area A_L per lipid; the curves connect 10 ps running averages. The experimental values[4] are plotted as straight gray lines.

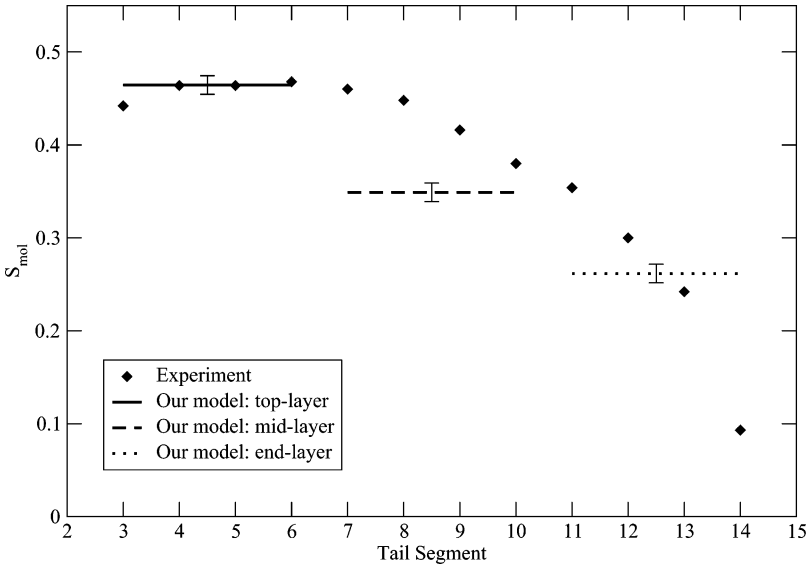

Figure 4. Tail order parameters. The estimated segmental order parameters[79] from experiment[5] are superimposed on our simulation results obtained by averaging over layers of tail sites as defined in the text. Standard errors are reported.

construction) cannot capture this feature as the four consecutive methyl groups at the end of each tail, represented by a single rigid ellipsoid, are assumed to be aligned. From the distance between the maxima of the profile, we compute a membrane thickness of $d_{HH} = 3.71 \pm 0.02$ nm, close to the experimental value[4] of 3.53 nm. Single-site profiles are shown in Figure 6. We observe broad peaks, significant headgroup hydration, and water penetration down to the glycerol region. These findings are consistent with AL simulation data.[22−24]

Headgroup dipole. We define the headgroup dipole moment as $\vec{\mu}_{HG} = q\vec{d}$, with $\vec{d}$ as the instantaneous vector connecting the phosphate to the choline mass center and q as the (equal) absolute magnitude of each headgroup charge. Owing to the lack of experimental data for the headgroup dipole of DMPC, we compare our model with experiments on dipalmitoylphosphatidylcholine (DPPC) bilayers. Apart from slightly longer tails (two more carbons), DPPC is identical to DMPC; also, the experiments considered[83,84] were carried out on fully hydrated bilayers in the fluid phase, under the same conditions as those in our simulation. Therefore, it is reasonable to compare our results for DMPC with these experimental data for DPPC. We calculate a dipole magnitude of $\mu_{HG} = 16.1 \pm 0.1$ D, broadly consistent with the experimental estimate[83] for DPPC of 18.7 D. As for the orientation, the headgroup dipole of our model is inclined, on average, by 92.3° from the membrane normal, marginally pointing toward the bilayer interior. Experiment on fluid-phase DPPC estimated the preferred conformation at ≈72° from the membrane normal, hence slightly pointing toward the water phase.[84] Despite a small discrepancy regarding the average angle, our result agrees with experiment by describing the headgroup dipole as being roughly parallel to the membrane plane.[84] A recent AL simulation study of DMPC also reported the headgroup dipole to lie essentially flat on the bilayer plane, the average angle being estimated at 72.3° from the interface normal.[23]

Mechanical Properties. *Compressibility Moduli.* The area compressibility K_A can be computed from simulation as $K_A = k_BTA/\sigma^2(A)$, A and $\sigma^2(A)$ being, respectively, the mean and mean-squared fluctuation of the interfacial area. We have calculated for our model $K_A = 297 \pm 22$ dyn/cm, a value consistent with the experimental measurement[7] of 234 dyn/cm. The volume compressibility modulus K_V can be computed as $K_V = k_BTV/$

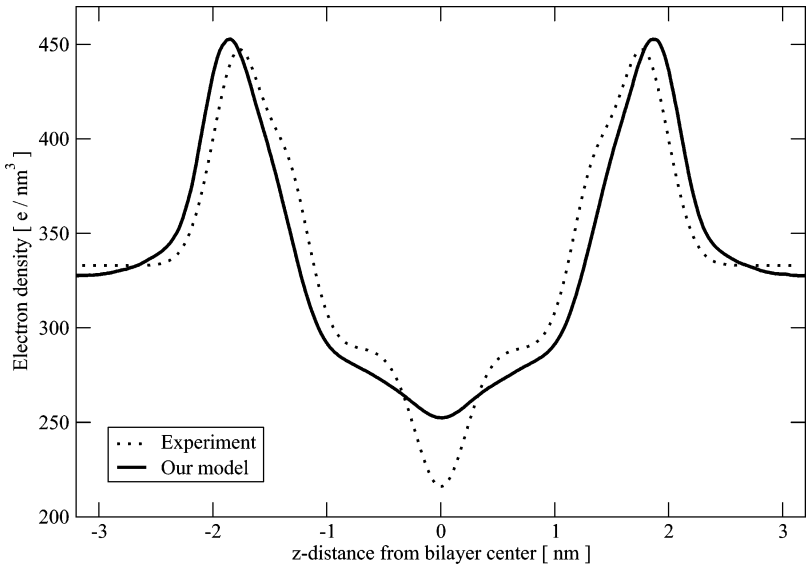

Figure 5. Total electron density profile. The distribution calculated with our model is superimposed on the profile obtained from experiment.[4]

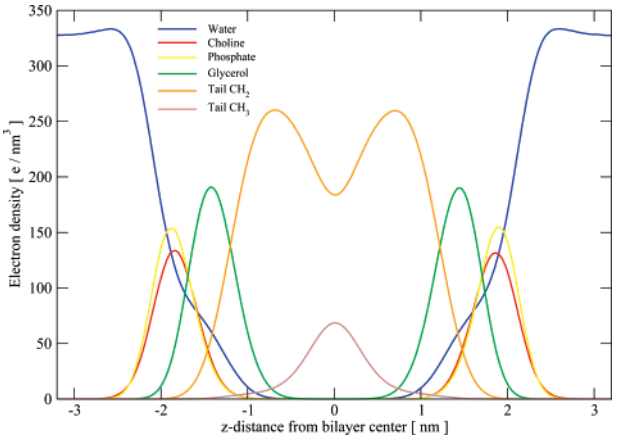

Figure 6. Single-site electron density profiles. Distributions are displayed for each site of our model. For the tail sites, electrons belonging to the CH_2 groups have been differentiated from the ones belonging to the terminal CH_3 group.

$\sigma^2(V)$, V and $\sigma^2(V)$ being, respectively, the mean and mean-squared fluctuation of the volume of the simulation region. We have calculated for our model $K_V = 13.7 \pm 0.2$ kbar, consistent with the experimental range of 10−30 kbar reported as typical for fluid-phase phospholipid bilayers.[1]

Bending Rigidity Modulus. The bilayer bending modulus κ^b can be related to the area compressibility modulus K_A via[7] $\kappa^b = K_A d_t^2/24$, the "effective" bilayer thickness d_t being $d_t = d_{HH} - 1$ nm, with d_{HH} as the peak-to-peak distance in the electron density profile. Using K_A and d_{HH} from our previous results, we obtain $\kappa^b = 21.9 \pm 1.6 k_B T$. Experiments have measured $16.7 k_B T$ from X-ray data,[85] $13.5 k_B T$ from pipet aspiration,[7] $31.4 k_B T$ from thermally excited shape fluctuation,[86] and $32.1 k_B T$ from all-optical measurement.[87] Our estimate lies inside the range of the experimental values.

Lateral Pressure Profile. The transmembrane lateral pressure profile $\pi(z)$ of our model, calculated by a standard procedure,[30,33] is reported in Figure 7. Distinctive features can be highlighted and related to their molecular origin. Corresponding to the interfacial water regions, at the left and right extremes of the profile, the net lateral pressure is almost zero, as it should be for bulk water at mechanical equilibrium. In fact, it is possible to observe a slightly positive value, which indicates repulsive interactions; these arise from the partial alignment of water dipoles as a consequence of the strong membrane electric field (as analyzed in the following section on water polarization) and the disturbance of interfacial water due to the nearby lipid headgroups (with occasional headgroup protrusions into the water phase). Upon entering the membrane, at the headgroup region, we observe large positive lateral pressures, with a peak magnitude of ≈370 atm, which reflect a strong desire of the bilayer interfacial area to expand. This results from repulsive interactions between the headgroups due to steric, electrostatic, and hydration forces.[1] At the polar/apolar interface, roughly corresponding to the lipid glycerol groups, the profile is characterized by deep troughs of lateral pressure, with minimum values of ≈−650 atm (Figure 7). Here, the interfacial tension tries to contract the bilayer to minimize the exposure of the hydrocarbon core to the polar environment. In the bilayer hydrocarbon interior, the pressure profile displays positive values. The tight lipid packing conditions result in stretched tails with respect to isolated "free" tails; the corresponding entropy loss causes significant intertail repulsion.[88] In particular, the hydrocarbon region is characterized by three local maxima and two local minima. Two outer maxima, of peak magnitude ≈ 180 atm, are located corresponding to the top segments of the lipid tails; high ordering here (see Figure 4) is indicative of high entropy loss, which results in large repulsive forces. The two pressure minima are observed corresponding to the midtail segments; in this region, the packing-related entropy loss is relatively small since the connectivity to neighboring segments already limits the midtail conformational entropy in free tails. A broad lateral pressure maximum, of peak magnitude ≈ 200 atm, is located at the very center of the bilayer (Figure 7). Here, the ordering is minimal (see again Figure 4), and hence, the presence of such large repulsive forces might seem unjustified. However, the relative entropy loss of the tail ends in the hydrocarbon core, with respect to free tails, is predicted to be maximal,[89] thus leading to sharp pressure increases toward the bilayer center. Experimental investigation of the lateral pressure distribution is extremely difficult; the few attempts made to date provide qualitative and partial pictures for the hydrocarbon region only.[9,13] Unfortunately, the lateral pressure inside the DMPC bilayers has never been experimentally investigated. However, the pressure distribution has been probed for dioleylphosphatidylcholine (DOPC) bilayers.[9] DOPC tails are slightly longer than DMPC (18 vs 14 carbons) and contain one double

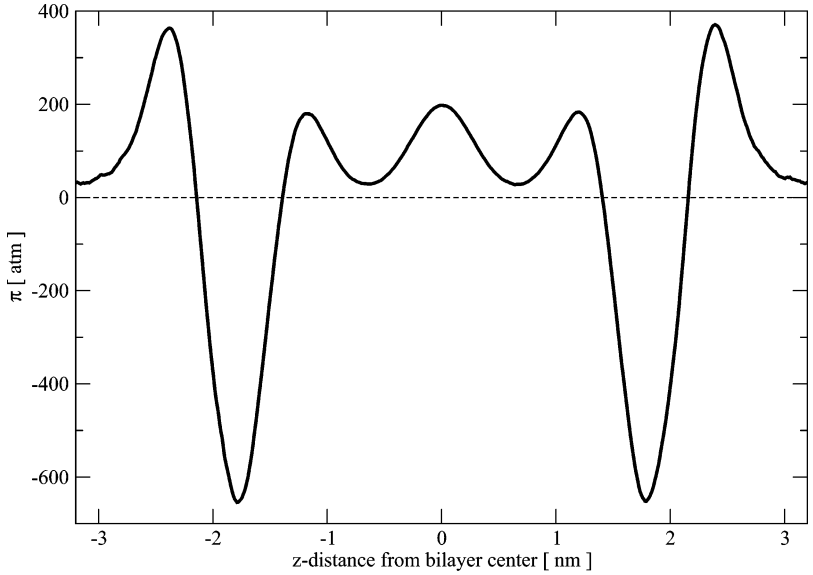

Figure 7. Lateral pressure profile.

bond (or unsaturation), whereas DMPC is fully saturated. The headgroup and glycerol regions are identical for the two species. The experiment[9] was carried out with fully hydrated fluid-phase bilayers, as in our simulation. Overall, it seems reasonable to compare our results for DMPC with the data for DOPC. The experimental data indicate that the hydrocarbon tails generate positive pressures nonuniformly distributed; in particular, local minima roughly at mid-depth along the tails of each leaflet were observed.[9] The qualitative experimental picture is therefore consistent with our calculation. Our profile can also be compared to the distributions obtained from AL bilayer models of a variety of phospholipid species.[30−36] We note a general agreement on the number and locations of the pressure peaks and troughs. In particular, the midtail minima are also reproduced by these models; they are observed for fully saturated[30−35] as well as for unsaturated[33−36] lipids. In terms of magnitude, AL models are broadly consistent with ours in the peak values recorded. In particular, peak pressures recorded for fully saturated lipids[30−35] are on the order of 200 to 600 atm for the headgroup maxima, −500 to −1000 atm for the polar/apolar interfacial troughs, and 200 to 300 atm for the central peak. Our results lie inside of these intervals. The only AL pressure profile DMPC available[31] displays the qualitative features present in our profile, although the peak magnitudes are slightly different. The AL profile[31] is rather noisy, and it was computed from a relatively short run (14.3 ns after only 5 ps of equilibration). Hence, it is probably undersampled and not fully converged. Also, the membrane area was held fixed, whereas in our simulation, the *xy* interfacial plane fluctuated according to the lateral components of the pressure tensor. It is therefore not appropriate to compare in detail our profile to that AL curve.[31] Regarding the other specific CG models developed to date, the lateral pressure profile has been calculated so far only once, for a DPPC bilayer;[90] there are issues, however, with the reported data, in that the CG pressure profile[90] does not feature the midtail minima and displays magnitudes that are markedly different from the other published AL results[30,34,35] for DPPC bilayers. Pressure profiles have also been computed from particle-based simulations of generic coarse-grain models.[91−98] It has been argued[32] that the level of simplification of these models (which do not incorporate electrostatics and contain highly simplified water representations) makes their pressure profile predictions questionable. In fact, some qualitative features are captured, although none of these models reproduce a central pressure maximum as observed in our profile and in the AL studies; central minima of nearly zero[91−94] or negative [95−98] magnitude are instead reported. Predictions of the pressure profile have also been obtained by analytical theory.[89,99−101] These methods typically consider only the tail region, and they assume uniform density. Two of these models[89,101] reproduce the midtail minima. With one exception,[89] the pressure profiles obtained by analytical theory do not feature the central maximum corresponding to the tail ends.

Membrane Curvature Elasticity. In the popular formalism developed by Helfrich,[16−18] the surface curvature elastic energy per unit area g is expressed as $g = \kappa(c_1 + c_2 - c_0)^2/2 + \kappa_G c_1 c_2$, with κ as the bending rigidity, c_1 and c_2 as the (local) principal curvatures, c_0 as the spontaneous (or intrinsic) curvature, and κ_G as the Gaussian curvature modulus. In the following sections, we will calculate the constants c_0 and κ_G by evaluating the first and second integral moments of the pressure profile over each monolayer.[88] The final values and standard errors are estimated from four separate averages, two (one for each monolayer) for each of the two consecutive 100 ns measurement blocks. Similar calculations have been previously performed by analytical theory,[99,102] with a generic CG model,[103,104] and with AL models,[33,35] although not for DMPC. Experimental data for DMPC are also lacking. However, we will be able to compare our results to experimental data for similar lipids and to general theoretical predictions.

Torque Tension and Spontaneous Curvature. We have calculated the first integral moment P_1 of the lateral pressure profile π as

$$P_1 = \int_0^h z\pi(z)\mathrm{d}z$$

where $z = 0$ at the center of the bilayer and $z = h$ in the water phase.[88] In particular, we have integrated the pressure profile over each of the two monolayers, with $z = 0$ and $\pm h$, h being half of the z dimension of the simulation region. The first moment of the lateral pressure is also called the torque tension τ^m, with the superscript "m" indicating "monolayer". We have calculated a monolayer torque tension $\tau^m = P_1 = -0.020 \pm 0.003 k_B T/\text{Å}$. We can then write[99] $\tau^m = \kappa^m c_0^m$, with κ^m and c_0^m being the monolayer bending rigidity and spontaneous curvature,

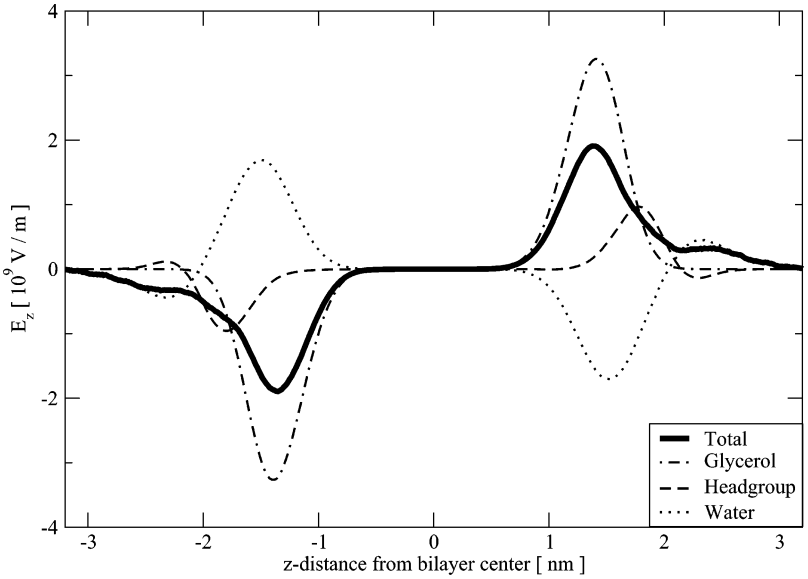

Figure 8. Transbilayer electric field. The *z* projection of the total transmembrane electric field is plotted together with single-site profiles.

respectively. Considering that[11] $\kappa^m = \kappa^b/2$, we obtain a monolayer spontaneous curvature of $c_0^m = -0.018 \pm 0.003$ nm^{-1}. The spontaneous curvature has been measured for a number of type-II lipids, that is, lipids forming inverted nonlamellar structures; typical values in the range of -0.05 to -1 nm^{-1} have been reported.[11] Lower absolute values are expected for bilayer-forming, type-0 lipids, such as DMPC. Our estimate is therefore reasonable.

Gaussian Curvature Modulus. The monolayer Gaussian curvature modulus can be determined as

$$\kappa_G^m = -\int_0^h (z - \xi)^2 \pi(z) \mathrm{d}z$$

ξ being the distance to the pivotal surface, defined as the surface at which there is no change in the molecular cross-sectional area upon bending.[11] Defining the second integral moment P_2 of the lateral pressure profile as

$$P_2 = \int_0^h z^2 \pi(z)\, \mathrm{d}z$$

we can rewrite the expression for the Gaussian curvature modulus as $\kappa_G^m = 2\xi P_1 - P_2$, P_1 being the first moment. The pivotal surface ξ has been experimentally identified close to the polar/apolar interface.[105] Considering the lateral pressure profile (Figure 7), we assume the polar/apolar interfaces of the two monolayers to be located at the two main troughs of the curve. In fact, the global minima of the pressure profile identify the regions of largest surface tension, situated at the hydrophobic/hydrophilic interfacial regions. Hence, by computing the half-distance between the global minima of the pressure profile, we set $\xi = 1.79$ nm. The second integral moment of the pressure profile from simulation is $P_2 = 5.3 \pm 0.1 k_B T$. With P_1 and ξ as defined previously, we finally obtain $\kappa_G^m = -5.4 \pm 0.1 k_B T$. It has been shown[105] that the monolayer Gaussian curvature modulus is generally related to the bending rigidity according to $-1 < \kappa_G^m/\kappa^m < 0$; this prediction has been confirmed experimentally.[11] The more stringent relation $\kappa_G^m/\kappa^m \approx -0.8$ has also been proposed.[18] For our model, assuming $\kappa^m = \kappa^b/2$,[11] we calculate $\kappa_G^m/\kappa^m \approx -0.5$, a value consistent with the reported theoretical predictions. We have also estimated the bilayer Gaussian curvature modulus as[17] $\kappa_G^b = 2(\kappa_G^m - 2\kappa^m c_0^m \xi) = -10.9 \pm 2.3 k_B T$.

Electrostatic Properties. *Electric Field.* We have computed the transbilayer electric field by integrating the charge density of the system along the bilayer normal.[106] The *z* projection of the electric field as a function of the position along the bilayer normal is reported in Figure 8; the total profile is displayed together with single-site profiles of the various charged groups. The calculated magnitude of the total electric field within the membrane is enormous, with local values on the order of $\approx 10^9$ V/m. Although no direct experimental measure is available, such a large figure is expected,[107] considering the magnitude of the dipole potential (see next section). The total electric field arises predominantly from the glycerol−ester dipoles through their alignment along the interface normal. The headgroup contribution is relatively small; in fact, the headgroup dipole lies almost parallel to the membrane plane, and hence, despite its large magnitude, its projection along the normal and, consequently, the *z* component of the electric field will be small, on average. A significant contribution to the net total field is due to interfacial water; water dipoles generate a strong field, which counteracts the total field to lower the overall magnitude. We have further investigated interfacial water by quantifying water ordering. In particular, we have calculated the transbilayer water polarization profile as the first-rank $P_1(z)$ order parameter[65] of the water dipoles with respect to the interface normal. To better represent the physical significance of interfacial water ordering, we have also computed the density-weighted profile by multiplying $P_1(z)$ by the water number density profile ρ_W (deduced from the electron density of Figure 6). The density-weighted water polarization profile is shown in Figure 9; the correlation with the water electric field (Figure 8) is evident.

Dipole Potential. We have calculated the electrical potential profile $\Psi(z)$ by integrating the electric field along the interface normal.[106] Figure 10 reports the total transmembrane electric potential together with single-site profiles. The molecular origin of the membrane dipole potential can be clearly identified; according to our results, the overall potential largely originates from the glycerol groups. Water ordering generates a negative potential that lowers the overall value, whereas the headgroup contribution is comparatively small. The total membrane dipole Ψ_d for our model, measured in the hydrocarbon core with respect to the water phase, is $+1.57 \pm 0.03$ V. Experimentally, a value of $+0.45$ V for DMPC was obtained with the monolayer method.[108] Cryo-EM experiments have recently estimated a

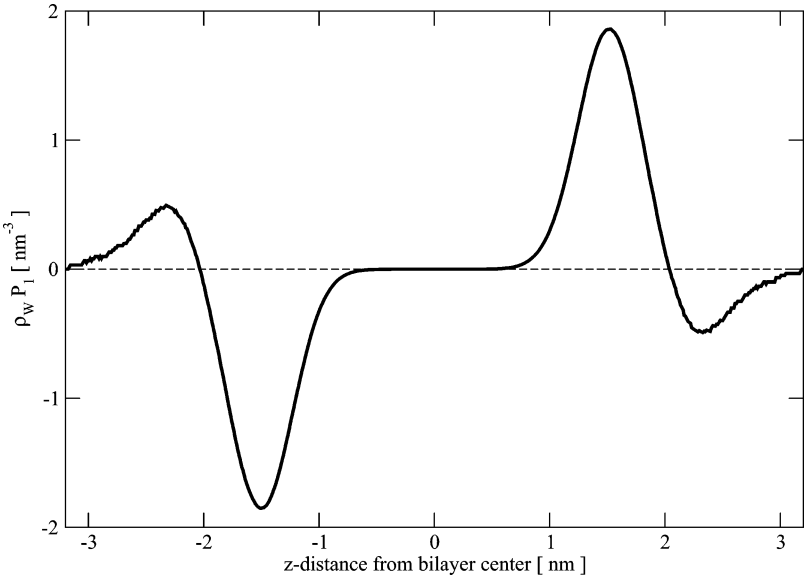

Figure 9. Transbilayer water polarization profile. The first-rank order parameter P_1 of the water dipoles with respect to the z axis unit vector is weighted by the water number density ρ_W. Considering the frame of reference employed, the interface normal originates at the center of the system and is oriented along the z axis. Hence, positive values in the left half of the water polarization profile correspond to water dipoles oriented toward the bilayer interior, whereas negative values correspond to water dipoles oriented toward the water phase. For the right half of the curve, the convention is reversed.

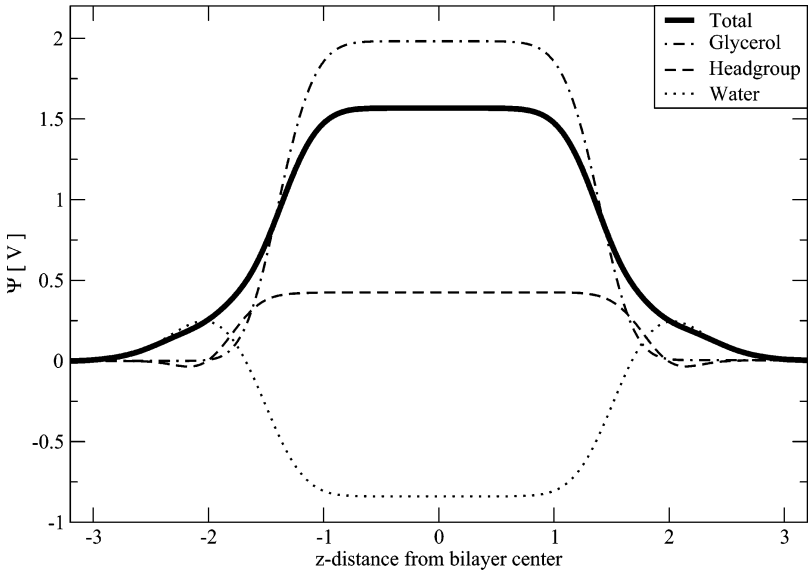

Figure 10. Electrical potential profile. The total transmembrane potential is plotted together with single-site profiles.

magnitude of +0.51 V for a diphytanoylphosphatidylcholine (DPhPC) bilayer;[8] this result can be reasonably considered as representative for ester−PC lipid bilayers in general (thus including DMPC) due to the presence of the same charged groups (glycerol−ester and headgroup). Our model correctly predicts the sign of the dipole potential, although the magnitude is larger than those estimated experimentally. Part of the reason for the discrepancy observed is specific to our model. In our simulation, the headgroup dipole points, on average, slightly toward the bilayer interior, thus generating a small positive contribution to the dipole potential (Figure 10). As already noted, experiments suggest instead an orientation slightly pointing toward the water phase,[84] which would give rise to a negative contribution to the dipole potential. A possible solution, which we are indeed considering, involves introducing an angular bonded term, of the form typically present in both AL and CG force fields, to restrain the headgroup dipole to a configuration more similar to that of the experiment; this would yield a more realistic headgroup configuration and, in turn, a lower total potential. It is worth pointing out that large values for the membrane dipole have also been obtained with a number of AL models; [27−29] the overestimation of internal electrical potentials might be partly due to a general weakness of nonpolarizable force fields.

Dynamics. *Lipid Lateral Diffusion.* We have calculated the lipid lateral diffusion coefficient using the Einstein expression,[72] as is standard practice in membrane simulations.[21−23] Figure 11 shows the lipid lateral diffusion coefficient D_{lat} computed for two different measurement times. In particular, the diffusion coefficient measured on a subnanosecond scale is reported in the top panel of Figure 11; at 0.5 ns, a representative value of $\approx$60 nm$^2/\mu$s can be observed. This result is consistent with those obtained from experimental methods such as quasi-elastic neutron scattering,[109] which measure lipid displacements over time periods of less than a nanosecond and yield short-range diffusion constants in the range of 10−100 nm$^2/\mu$s. In the bottom

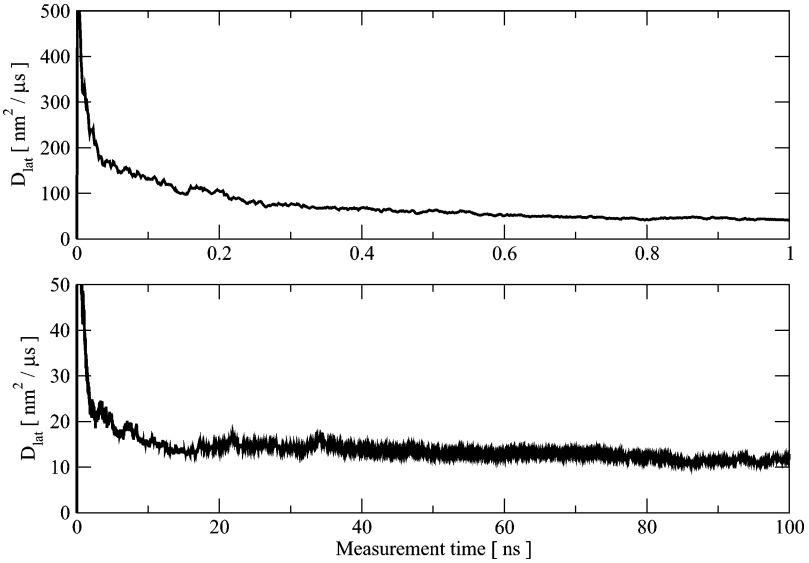

Figure 11. Lateral diffusion coefficients of lipid mass centers calculated using the Einstein relation as a function of the measurement time. The top panel (1 ns temporal scale) refers to short-range diffusion, whereas the bottom panel (100 ns temporal scale) refers to long-range diffusion.

panel of Figure 11, we report the diffusion measurement over a 100 ns scale; the converged value is 12 ± 3 nm$^2/\mu$s. This result is consistent with the value of 9 nm$^2/\mu$s measured by pulsed field gradient NMR spectroscopy.[6] Our diffusion results, both for short and long time scales, are also consistent with recent AL simulation data.[21] The reason why lipid diffusion rates are different over short and long ranges can be understood by considering the free-volume theory.[110] According to the free-volume model, lateral diffusion occurs by discrete jumps of lipid molecules into nearby vacancies formed by lateral density fluctuations; in between jumps, a lipid molecule spends a relatively long time rattling in a cage formed by its neighbors. Over short (<1 ns) time scales, the diffusion coefficient is high because it is determined by the fast short-range lipid motion mainly due to a "rattling-about" behavior. However, considering longer times, this rattling motion averages out, yielding no net displacement. The true, long-range diffusion coefficient is determined by the lipid jumps, which give rise to effective displacement over longer (>10 ns) time scales. From our simulation, we can directly visualize the lipid diffusion mechanism by recording single-lipid trajectories and projecting them onto the bilayer plane. Figure 12 reports the mass center lateral motion of selected lipids over a 100 ns time window; the "rattling" pattern, accompanied by occasional jumps, is clearly observable. To our knowledge, there are no experimental data directly showing the free-volume diffusive mechanism at this level of resolution. Also, no explicit single-lipid trace has been reported for other CG models yet. Results similar to ours have been obtained using AL models,[22,25] although they are from shorter simulations (10−50 ns).

Water Permeation. By simulating over relatively long times, we observe statistically significant numbers of water molecules penetrating through the bilayer from one water phase to the other. In particular, over 900 ns, we have detected 208 crossing events, 107 along the z axis positive direction and 101 along the opposite (negative) direction. We have then computed the water permeability coefficient using Fick's law. The water concentration gradient is calculated as $\Delta C_W = C_W^{\text{waterphase}} - C_W^{\text{hydrocarboncore}} = 33$ nm^{-3}, assuming $C_W^{\text{hydrocarboncore}} = 0$ nm^{-3}. Considering the interfacial area A and the unidirectional flux of water J_W, we computed a permeability coefficient of $P_W = J_W/\Delta C_W A = 92 \pm 4$ μm/s, in good agreement with the experimental estimate[2] of 70 μm/s. Such a calculation has been previously reported once for another CG model.[40] Passive water transport has never been quantified with AL models due to the very demanding computational efforts required to simulate long trajectories. For example, in a recent AL study,[34] 4 phosphatidylcholine bilayers, each comprising 128 lipids, have been simulated for 50 ns. In the four simulations, two, four, six, and seven crossing events were observed. It is evidently not possible to attempt an estimation of the permeability coefficient on the basis of such poor statistics.

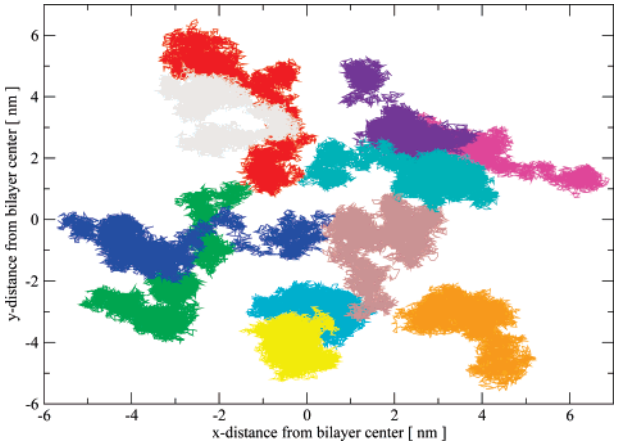

Figure 12. Mass center traces of selected lipids over a 100 ns time window. Each trace, identified by a different color, represents the mass center motion of a single lipid projected onto the *xy* plane.

Discussion

We have presented a new specific CG model for biological membrane systems. To some extent, our approach is similar to a number of CG membrane models that have recently been developed.[40−45] However, three main characteristics set our model apart from the other CG methodologies developed to date: explicit incorporation of the main electrostatics, realistic description of water, and use of anisotropic potentials to accurately capture lipid shape.

We employed our methodology to simulate a fluid-phase DMPC bilayer. The model was parametrized to reproduce basic

experimental data (volume and area per lipid, order parameters) and the self-assembly process. The time scale and overall self-aggregation mechanism are consistent with the available atomic-level data.[20] All major physical features of our self-assembled bilayer system were then quantitatively evaluated; we stress the fact that these properties did not directly enter the parametrization process. Structural results compared well with corresponding experimental data. In particular, the total electron density profile matched the curve obtained via experiment (Figure 5), and single-site profiles showed characteristic broad distribution peaks (Figure 6), consistent with the notion of fluid-phase lipid bilayers being highly disordered yet distinctly stratified systems.[3] The headgroup dipole moment was also analyzed; the experimental magnitude was reproduced, while the average orientation was found to be slightly different from that observed experimentally.

A thorough mechanical analysis was performed. First, compressibility moduli were evaluated. The area compressibility modulus describes the response of the bilayer surface area to an isotropic tension, whereas the volume (or bulk) compressibility modulus describes the response of the bilayer volume to uniform hydrostatic pressure.[1] Both parameters represent fundamental mechanical properties. The compressibilities computed for our model proved consistent with experimental measurement. The transbilayer lateral pressure profile was calculated (Figure 7). The profile was thoroughly analyzed; every feature was described and related to its molecular origin. Although no quantitative experimental data is available to confirm our result, the profile of our model seems very reasonable; it shows the qualitative features obtained from experiments performed on similar systems,[9] and both shape and magnitude are consistent with AL simulation data.[30−36] We then analyzed our simulation according to the elasticity theory developed by Helfrich. [16−18] The Helfrich formula, valid both for a monolayer and a bilayer, characterizes the spontaneous shape of interfaces, and it predicts the stored energies that accumulate as a result of deviations from the spontaneous shape. In particular, from the first integral moment of the pressure distribution, we determined the monolayer torque tension, which characterizes the curvature elastic stress,[111,112] and the spontaneous curvature, which quantifies the tendency to curl and to form different phases.[17] Both these parameters are believed to specifically control protein function, membrane stability, phase behavior, and fusion.[111,112] Our model proved able to correctly predict a monolayer curvature typical of type-0, bilayer-forming lipids for DMPC. Through the second integral moment of the pressure profile, we computed the Gaussian curvature modulus, which, in general, describes the energy required to change the Gaussian curvature of a surface. From a biophysical perspective, the Gaussian curvature modulus sensitively affects the energy of intermediates in phase transitions and fusion of phospholipid bilayers,[113] and it is also predicted to strongly influence the membrane-mediated interactions between embedded proteins.[104] Our calculation proved in agreement with theoretical predictions.[11,18] It is important to highlight that the consistent results obtained for the curvature elastic parameters provide further confidence that the pressure profile obtained with our model is quantitatively credible.

Electrical properties were also investigated. In particular, we studied the membrane dipole potential and associated transbilayer electric field. Our model correctly predicted the sign of the membrane potential, the magnitude being larger than the experimental estimate. Notably, we addressed an important issue which cannot be directly studied in real systems and which still represents an open question,[107] the molecular origin of the dipole potential. In particular, by separating individual contributions, we could identify the glycerol−ester dipoles as the major contributors to the electric field and dipole potential (Figures 8 and 10), and we could quantify the strong influence of interfacial water ordering (Figure 9). Both these observations confirm hypotheses based on experimental data.[114,115]

TABLE 2: Physical Parameters of the Fluid-Phase DMPC Phospholipid Bilayer[a]

parameter	our model	experiment[b]
V_L [nm^3]	1.104 ± 0.002	1.101[4]
A_L [nm^2]	0.594 ± 0.003	0.606[4]
d_{HH} [nm]	3.71 ± 0.02	3.53[4]
S_{mol}	0.36 ± 0.01	0.38[5,79]
μ_{HG} [D]	16.1 ± 0.1	18.7[83,c]
θ_{HG} [deg]	92.3 ± 0.1	≈72[84,c]
K_A [dyn/cm]	297 ± 22	234[7]
K_V [kbar]	13.7 ± 0.2	10 to 30[1]
κ^b [k_BT]	21.9 ± 1.6	13.5,[7] 16.7,[85] 31.4,[86] 32.1[87]
τ^m [k_BT/Å]	−0.020 ± 0.003	na
c_0^m [nm^{-1}]	−0.018 ± 0.003	≈0
κ_G^m [k_BT]	−5.4 ± 0.1	−10.9 to 0[11]
κ_G^b [k_BT]	−10.9 ± 2.3	na
Ψ_d [V]	1.57 ± 0.03	0.45,[108] 0.51[8,d]
D_{lat} [nm^2/μs]	12 ± 3	9[6]
P_W [μm/s]	92 ± 4	70[2]

[a] Abbreviations: V_L = volume per lipid, A_L = area per lipid, d_{HH} = bilayer thickness, S_{mol} = segmental order parameter, μ_{HG} = magnitude of the headgroup dipole, θ_{HG} = angle between the headgroup dipole and the bilayer normal, K_A = area compressibility, K_V = volume compressibility, κ^b = bilayer bending rigidity, τ^m = monolayer torque tension, c_0^m = monolayer spontaneous curvature, κ_G^m = monolayer Gaussian curvature, κ_G^b = bilayer Gaussian curvature, Ψ_d = dipole potential, D_{lat} = lipid lateral diffusion, P_W = water permeability, na = not available. [b] Superscripted numbers are references. [c] Fluid-phase DPPC. [d] Fluid-phase DPhPC.

Realistic lipid diffusion was also simulated; our results, both for short-range and long-range coefficients, proved consistent with experiments (Figure 11). Furthermore, single-lipid diffusion trajectories were extracted (Figure 12). We observed a "rattling and jumping" behavior of the kind predicted by the free-volume theory[110] and simulated in AL studies.[22,25] Finally, long-time simulation (almost 1 μs) allowed the spontaneous permeation of water molecules to be observed and quantified; we measured a permeability coefficient consistent with experiment.

The entire set of quantitative results obtained from our simulation is collected in Table 2, along with the corresponding experimental data. In general, experimental investigation on phospholipid bilayers suggests that the properties of membranes are governed by basic, purely physical principles.[3] Our model is a demonstration of the validity of this view; we have consistently reproduced experiments with a simple model that includes only the fundamental physics.

There are potentially many future extensions to the model presented. In fact, preliminary investigations into the modeling of different lipid species (such as DOPC) are being carried out. Cholesterol is also a primary candidate for future inclusion in our CG model; the Gay−Berne potential can allow cholesterol to be modeled accurately and efficiently with disk-like sites.

A unique and very promising aspect of our CG strategy is the straightforward compatibility with AL models; the potentials present in our force field can be readily mixed with AL force fields. In fact, electrostatic and van der Waals interactions are represented consistently by our CG model and standard AL models using Coulombic and Lennard-Jones potentials. Our model also comprises the anisotropic Gay−Berne potential, which can be seen as a generalization of the Lennard-Jones

potential. Gay−Berne and Lennard-Jones models can be mixed through a generalized formalism,[58] as we have already done to describe headgroup−tail and water−tail interactions. Recent work in our group has provided further evidence of the validity of our multiscale approach; in that study,[116] water−octane partition coefficients for a range of solutes were calculated by Monte Carlo simulations. Octane molecules have been modeled as pairs of Gay−Berne ellipsoids connected by a harmonic spring using the parameters developed here for the lipid hydrocarbon region, water has been represented with the SSD potential, and the solutes have been represented with an all-atom force field. This mixed AL−CG study has yielded results in good agreement with experimental data, using a fraction of the computational time needed by corresponding AL models. Furthermore, we are currently conducting AL−CG simulations where small organic molecules, described at the all-atom level using standard force field parameters, are inserted across our CG bilayer. In particular, we are performing the same investigation reported in a previous AL study,[26] where molecular dynamics simulations were used to calculate transmembrane free-energy profiles and permeability coefficients of eight small organic molecules. Preliminary results confirm the validity of our method; the data obtained from the AL−CG simulations are consistent with the corresponding AL results,[26] while the computation time is reduced by 2 orders of magnitude. Overall, it is clear how our approach can allow the efficient multiscale mixing of CG and AL models, the latter employed to represent molecules where fine chemical detail is important, such as drugs or membrane proteins.

Conclusion

We have reported the development of a new coarse-grain model for biomembranes and its application to the study of the most important physical properties of a representative fluid-phase phospholipid bilayer. The model has proved capable of consistently and quantitatively reproducing a large number of experimental observables, in terms of structure, elasticity, electrostatics, and dynamics. In this work, for the first time, a coarse-grain membrane model has yielded quantitative data for the headgroup dipole, Gaussian curvature modulus, electric field and electrostatic potential profiles, interfacial water ordering, short-range and long-range lateral diffusion coefficients, single-lipid diffusive paths, and spontaneous permeation of explicit water. Molecular-level insights into crucial membrane properties and mechanisms have been obtained and rationalized. This study generally demonstrates that the fundamental behavior of lipid bilayers does not depend on fine chemical detail but on basic physical interactions. The direct compatibility of our model with standard atomic-level representations allows the study of problems where a multiscale approach is desirable.

Acknowledgment. This work has been funded by Johnson & Johnson, Janssen Pharmaceutica. Membrane snapshots (Figure 2) were generated using visualization software written by Dr. Robert J. Gledhill. The experimental electron density profile (Figure 5) was kindly provided by Professor John F. Nagle. We thank Dr. Julien Michel and Professor George S. Attard for stimulating discussion.

References and Notes

(1) Cevc, G.; Marsh, D. *Phospholipid Bilayers—Physical Principles and Models*, 1st ed.; John Wiley & Sons: New York, 1987.

(2) Bloom, M.; Evans, E.; Mouritsen, O. G. *Q. Rev. Biophys.* **1991**, *24*, 293.

(3) Mouritsen, O. G. *Life—As a Matter of Fat. The Emerging Science of Lipidomics*, 1st ed.; Springer: Berlin, 2005.

(4) Kučerka, N.; Liu, Y. F.; Chu, N. J.; Petrache, H. I.; Tristram-Nagle, S. T.; Nagle, J. F. *Biophys. J.* **2005**, *88*, 2626.

(5) Douliez, J.-P.; Leonard, A.; Dufourc, E. J. *Biophys. J.* **1995**, *68*, 1727.

(6) Filippov, A.; Orädd, G.; Lindblom, G. *Langmuir* **2003**, *19*, 6397.

(7) Rawicz, W.; Olbrich, K. C.; McIntosh, T.; Needham, D.; Evans, E. *Biophys. J.* **2000**, *79*, 328.

(8) Wang, L.; Bose, P. S.; Sigworth, F. J. *Proc. Natl. Acad. Sci. U.S.A.* **2006**, *103*, 18528.

(9) Templer, R. H.; Castle, S. J.; Curran, A. R.; Rumbles, G.; Klug, D. R. *Faraday Discuss.* **1998**, *111*, 41.

(10) Starke-Peterkovic, T.; Turner, N.; Vitha, M. F.; Waller, M. P.; Hibbs, D. E.; Clarke, R. J. *Biophys. J.* **2006**, *90*, 4060.

(11) Shearman, G. C.; Ces, O.; Templer, R. H.; Seddon, J. M. *J. Phys.: Condens. Matter* **2006**, *18*, S1105.

(12) van den Brink-van der Laan, E.; Killian, J. A.; de Kruijff, B. *Biochim. Biophys. Acta* **2004**, *1666*, 275.

(13) Kamo, T.; Nakano, M.; Kuroda, Y.; Handa, T. *J. Phys. Chem. B* **2006**, *110*, 24987.

(14) Curnow, P.; Lorch, M.; Charalambous, K.; Booth, P. J. *J. Mol. Biol.* **2004**, *343*, 213.

(15) Mohr, J. T.; Gribble, G. W.; Lin, S. S.; Eckenhoff, R. G.; Cantor, R. S. *J. Med. Chem.* **2005**, *48*, 4172.

(16) Helfrich, W. *Z. Naturforsch., C: Biosci.* **1973**, *28*, 693.

(17) Seddon, J. M.; Templer, R. H. In *Structure and Dynamics of Membranes*; Lipowsky, R., Sackmann, E., Eds.; Elsevier: New York, 1995; pp 97−160.

(18) Marsh, D. *Chem. Phys. Lipids* **2006**, *144*, 146.

(19) Essex, J. W.; Hann, M. M.; Richards, W. G. *Philos. Trans. R. Soc. London, Ser. B* **1994**, *344*, 239.

(20) Marrink, S.-J.; Lindahl, E.; Edholm, O.; Mark, A. E. *J. Am. Chem. Soc.* **2001**, *123*, 8638.

(21) Wohlert, J.; Edholm, O. *J. Chem. Phys.* **2006**, *125*, 204703.

(22) Moore, P. B.; Lopez, C. F.; Klein, M. L. *Biophys. J.* **2001**, *81*, 2484.

(23) Högberg, C.-J.; Lyubartsev, A. P. *J. Phys. Chem. B* **2006**, *110*, 14326.

(24) Klauda, J. B.; Kučerka, N.; Brooks, B. R.; Pastor, R. W.; Nagle, J. F. *Biophys. J.* **2006**, *90*, 2796.

(25) Klauda, J. B.; Brooks, B. R.; Pastor, R. W. *J. Chem. Phys.* **2006**, *125*, 144710.

(26) Bemporad, D.; Essex, J. W.; Luttmann, C. *J. Phys. Chem. B* **2004**, *108*, 4875.

(27) Sachs, J. N.; Crozier, P. S.; Woolf, T. B. *J. Chem. Phys.* **2004**, *121*, 10847.

(28) Shinoda, K.; Shinoda, W.; Baba, T.; Mikami, M. *J. Chem. Phys.* **2004**, *121*, 9648.

(29) Song, Y. H.; Guallar, V.; Baker, N. A. *Biochemistry* **2005**, *44*, 13425.

(30) Lindahl, E.; Edholm, O. *J. Chem. Phys.* **2000**, *113*, 3882.

(31) Gullingsrud, J.; Babakhani, A.; McCammon, J. A. *Mol. Simul.* **2006**, *32*, 831.

(32) Patra, M. *Eur. Biophys. J.* **2005**, *35*, 79.

(33) Gullingsrud, J.; Schulten, K. *Biophys. J.* **2004**, *86*, 3496.

(34) Ollila, S.; Hyvönen, M. T.; Vattulainen, I. *J. Phys. Chem. B* **2007**, *111*, 3139.

(35) Ollila, O. H. S.; Róg, T.; Karttunen, M.; Vattulainen, I. *J. Struct. Biol.* **2007**, *159*, 311.

(36) Carrillo-Tripp, M.; Feller, S. E. *Biochemistry* **2005**, *44*, 10164.

(37) Muller, M.; Katsov, K.; Schick, M. *Phys. Rep.* **2006**, *434*, 113.

(38) Brannigan, G.; Lin, L. C. L.; Brown, F. L. H. *Eur. Biophys. J.* **2006**, *35*, 104.

(39) Orsi, M.; Sanderson, W.; Essex, J. W. In *Molecular Interactions—Bringing Chemistry to Life*; Hicks, M. G., Kettner, C., Eds.; Beilstein-Institut: Frankfurt, Germany, 2007.

(40) Marrink, S.-J.; de Vries, A. H.; Mark, A. E. *J. Phys. Chem. B* **2004**, *108*, 750.

(41) Lyubartsev, A. P. *Eur Biophys J.* **2005**, *35*, 53.

(42) Shelley, J. C.; Shelley, M. Y.; Reeder, R. C.; Bandyopadhyay, S.; Klein, M. L. *J. Phys. Chem. B* **2001**, *105*, 4464.

(43) Elezgaray, J.; Laguerre, M. *Comput. Phys. Commun.* **2006**, *175*, 264.

(44) Kranenburg, M.; Nicolas, J. P.; Smit, B. *Phys. Chem. Chem. Phys.* **2004**, *6*, 4142.

(45) Izvekov, S.; Voth, G. A. *J. Phys. Chem. B* **2005**, *109*, 2469.

(46) Lopez, C. F.; Moore, P. B.; Shelley, J. C.; Shelley, M. Y.; Klein, M. L. *Comput. Phys. Commun.* **2002**, *147*, 1.

(47) Marrink, S.-J.; Mark, A. E. *Biophys. J.* **2004**, *87*, 3894.

(48) Nielsen, S. O.; Lopez, C. F.; Ivanov, I.; Moore, P. B.; Shelley, J. C.; Klein, M. L. *Biophys. J.* **2004**, *87*, 2107.

(49) Marrink, S.-J.; Mark, A. E. *J. Am. Chem. Soc.* **2003**, *125*, 11144.

(50) Kranenburg, M.; Vlaar, M.; Smit, B. *Biophys. J.* **2004**, *87*, 1596.
(51) Pickholz, M.; Saiz, L.; Klein, M. L. *Biophys. J.* **2005**, *88*, 1524.
(52) Izvekov, S.; Voth, G. A. *J. Chem. Theory Comput.* **2006**, *2*, 637.
(53) Bond, P. J.; Sansom, M. S. P. *J. Am. Chem. Soc.* **2006**, *128*, 2697.
(54) Chang, R.; Ayton, G. S.; Voth, G. A. *J. Chem. Phys.* **2005**, *122*, 244716.
(55) Shi, Q.; Izvekov, S.; Voth, G. A. *J. Phys. Chem. B* **2006**, *110*, 15045.
(56) Gay, J. G.; Berne, B. J. *J. Chem. Phys.* **1981**, *74*, 3316.
(57) Whitehead, L.; Edge, C. M.; Essex, J. W. *J. Comput. Chem.* **2001**, *22*, 1622.
(58) Cleaver, D. J.; Care, C. M.; Allen, M. P.; Neal, M. P. *Phys. Rev. E* **1996**, *54*, 559.
(59) Golubkov, P. A.; Ren, P. *J. Chem. Phys.* **2006**, *125*, 064103.
(60) Liu, Y.; Ichiye, T. *J. Phys. Chem.* **1996**, *100*, 2723.
(61) Chandra, A.; Ichiye, T. *J. Chem. Phys.* **1999**, *111*, 2701.
(62) Fennell, C. J.; Gezelter, J. D. *J. Chem. Phys.* **2004**, *120*, 9175.
(63) Tan, M.-L.; Brooks, B. R.; Ichiye, T. *Chem. Phys. Lett* **2006**, *421*, 166.
(64) Price, S. L.; Stone, A. J.; Alderton, M. *Mol. Phys.* **1984**, *52*, 987.
(65) Allen, M. P.; Tildesley, D. J. *Computer Simulation of Liquids*, 1st ed.; Oxford Science Publications: New York, 1987.
(66) Darden, T.; York, D.; Pedersen, L. *J. Chem. Phys.* **1993**, *98*, 10089.
(67) Tobias, D. J. *Curr. Opin. Struct. Biol.* **2001**, *11*, 253.
(68) Fennell, C. J.; Gezelter, J. D. *J. Chem. Phys.* **2006**, *124*, 234104.
(69) Scott, H. L. *Curr. Opin. Struct. Biol.* **2002**, *12*, 495.
(70) Beck, D. A. C.; Armen, R. S.; Daggett, V. *Biochemistry* **2005**, *44*, 609.
(71) BRAHMS: a Biomembrane Reduced-ApproacH Molecular Simulator. http://www.personal.soton.ac.uk/orsi/brahms/, In-house molecular dynamics software, Essex group, University of Southampton.
(72) Rapaport, D. C. *The Art of Molecular Dynamics Simulation*, 2nd ed.; Cambridge University Press: New York, 2004.
(73) Dullweber, A.; Leimkuhler, B.; McLachlan, R. *J. Chem. Phys.* **1997**, *107*, 5840.
(74) http://moose.bio.ucalgary.ca/files/dmpc_npat.pdb (accessed April 2007), Biocomputing group, University of Calgary.
(75) Berendsen, H. J. C.; Postma, J. P. M.; van Gunsteren, W. F.; Di Nola, A.; Haak, J. R. *J. Chem. Phys.* **1984**, *81*, 3684.
(76) Harvey, S. C.; Tan, R. K. Z.; Cheatham, T. E., III. *J. Comput. Chem.* **1998**, *19*, 726.
(77) Brooks, B. R.; Bruccoleri, R. E.; Olafson, B. D.; States, D. J.; Swaminathan, S.; Karplus, M. *J. Comput. Chem.* **1983**, *4*, 187.
(78) Iridis is a Beowulf cluster based on AMD Opteron processors, running RedHat Enterprise Linux. http://www.soton.ac.uk/iss/computing/hpc/iridis/.
(79) Seelig, J.; Niederberger, W. *J. Am. Chem. Soc.* **1974**, *96*, 2069.
(80) Leach, A. R. *Molecular Modelling—Principles and Applications*, 2nd ed.; Prentice Hall: New York, 2001.
(81) Feenstra, K. A.; Hess, B.; Berendsen, H. J. C. *J. Comput. Chem.* **1999**, *20*, 786.
(82) Mills, R. *J. Phys. Chem.* **1973**, *77*, 685.
(83) Shepherd, J. C. W.; Büldt, G. *Biochim. Biophys. Acta* **1978**, *514*, 83.
(84) Akutsu, H.; Nagamori, T. *Biochemistry* **1991**, *30*, 4510.
(85) Chu, N.; Kučerka, N.; Liu, Y. F.; Tristram-Nagle, S.; Nagle, J. F. *Phys. Rev. E* **2005**, *71*, 041904.
(86) Méléard, P.; Gerbeaud, C.; Pott, T.; Fernandez-Puente, L.; Bivas, I.; Mitov, M. D.; Dufourcq, J.; Bothorel, P. *Biophys. J.* **1997**, *72*, 2616.
(87) Lee, C.-H.; Lin, W.-C.; Wang, J. *Phys. Rev. E* **2001**, *6402*, 020901.
(88) Ben-Shaul, A. In *Structure and Dynamics of Membranes*; Lipowsky, R., Sackmann, E., Eds.; Elsevier: New York, 1995; pp 359−401.
(89) Mukhin, S. I.; Baoukina, S. *Phys. Rev. E* **2005**, *71*, 061918.
(90) Marrink, S.-J.; Risselada, H. J.; Yefimov, S.; Tieleman, D. P.; de Vries, A. H. *J. Phys. Chem. B* **2007**, *111*, 7812.
(91) Xiang, T.-X.; Anderson, B. D. *Biophys. J.* **1994**, *66*, 561.
(92) Venturoli, M.; Smit, B. *Phys. Chem. Commun*. **1999**, *10*, 9/064721.
(93) Brannigan, G.; Brown, F. L. H. *J. Chem. Phys.* **2004**, *120*, 1059.
(94) Frink, L. J.; Frischknecht, A. L. *Biophys. J.* **2006**, *91*, 4081.
(95) Goetz, R.; Lipowsky, R. *J. Chem. Phys.* **1998**, *108*, 7397.
(96) Shillcock, J. C.; Lipowsky, R. *J. Chem. Phys.* **2002**, *117*, 5048.
(97) Brannigan, G.; Philips, P. F.; Brown, F. L. H. *Phys. Rev. E* **2005**, *72*, 011915.
(98) Frischknecht, A. L.; Frink, L. J. D. *Phys. Rev. E* **2005**, *72*, 041924.
(99) Szleifer, I.; Kramer, D.; Ben-Shaul, A.; Gelbart, W. M.; Safran, S. A. *J. Chem. Phys.* **1990**, *92*, 6800.
(100) Harries, D.; Ben-Shaul, A. *J. Chem. Phys.* **1997**, *106*, 1609.
(101) Cantor, R. S. *Biophys. J.* **1999**, *76*, 2625.
(102) Cantor, R. S. *Chem. Phys. Lipids* **1999**, *101*, 45.
(103) Brannigan, G.; Brown, F. L. H. *Biophys. J.* **2006**, *90*, 1501.
(104) Brannigan, G.; Brown, F. L. H. *Biophys. J.* **2007**, *92*, 864.
(105) Templer, R. H.; Khoo, B. J.; Seddon, J. M. *Langmuir* **1998**, *14*, 7427.
(106) Sokhan, V. P.; Tildesley, D. J. *Mol. Phys.* **1997**, *92*, 625.
(107) Clarke, R. J. *Adv. Colloid Interface Sci.* **2001**, *89*, 263.
(108) Lairion, F.; Disalvo, E. A. *Langmuir* **2004**, *20*, 9151.
(109) Tabony, J.; Perly, B. *Biochim. Biophys. Acta* **1991**, *1063*, 67.
(110) Vaz, W. L. C.; Almeida, P. F. *Biophys. J.* **1991**, *60*, 1553.
(111) Attard, G. S.; Templer, R. H.; Smith, W. S.; Hunt, A. N.; Jackowski, S. *Proc. Natl. Acad. Sci. U.S.A.* **2000**, *97*, 9032.
(112) Bezrukov, S. M. *Curr. Opin. Colloid Interface Sci.* **2000**, *5*, 237.
(113) Siegel, D. P.; Kozlov, M. M. *Biophys. J.* **2004**, *87*, 366.
(114) Flewelling, R. F.; Hubbell, W. L. *Biophys. J.* **1986**, *49*, 541.
(115) Gawrisch, K.; Ruston, D.; Zimmerberg, J.; Parsegian, V. A.; Rand, R. P.; Fuller, N. *Biophys. J.* **1992**, *61*, 1213.
(116) Michel, J.; Orsi, M.; Essex, J. W. *J. Phys. Chem. B*, in press.